ANL/CSE-13/29

Report Documenting the Speciation of Metals in Homogeneous Reactor Solutions: RERTR Milestone Report

Chemical Science and Engineering Division

About Argonne National Laboratory
Argonne is a U.S. Department of Energy laboratory managed by UChicago Argonne, LLC under contract DE-AC02-06CH11357. The Laboratory's main facility is outside Chicago, at 9700 South Cass Avenue, Argonne, Illinois 60439. For information about Argonne and its pioneering science and technology programs, see www.anl.gov.

DOCUMENT AVAILABILITY

Online Access: U.S. Department of Energy (DOE) reports produced after 1991 and a growing number of pre-1991 documents are available free via DOE's SciTech Connect (http://www.osti.gov/scitech/)

Reports not in digital format may be purchased by the public from the National Technical Information Service (NTIS):
U.S. Department of Commerce
National Technical Information Service
5301 Shawnee Rd
Alexandra, VA 22312
www.ntis.gov
Phone: (800) 553-NTIS (6847) or (703) 605-6000
Fax: (703) 605-6900
Email: **orders@ntis.gov**

Reports not in digital format are available to DOE and DOE contractors from the Office of Scientific and Technical Information (OSTI):
U.S. Department of Energy
Office of Scientific and Technical Information
P.O. Box 62
Oak Ridge, TN 37831-0062
www.osti.gov
Phone: (865) 576-8401
Fax: (865) 576-5728
Email: **reports@osti.gov**

Disclaimer
This report was prepared as an account of work sponsored by an agency of the United States Government. Neither the United States Government nor any agency thereof, nor UChicago Argonne, LLC, nor any of their employees or officers, makes any warranty, express or implied, or assumes any legal liability or responsibility for the accuracy, completeness, or usefulness of any information, apparatus, product, or process disclosed, or represents that its use would not infringe privately owned rights. Reference herein to any specific commercial product, process, or service by trade name, trademark, manufacturer, or otherwise, does not necessarily constitute or imply its endorsement, recommendation, or favoring by the United States Government or any agency thereof. The views and opinions of document authors expressed herein do not necessarily state or reflect those of the United States Government or any agency thereof, Argonne National Laboratory, or UChicago Argonne, LLC.

ANL/CSE-13/29

Report Documenting the Speciation of Metals in Homogeneous Reactor Solutions: RERTR Milestone Report

by
James Jerden, Jeffrey Fortner, and Dominique Stepinski
Chemical Science and Engineering Division, Argonne National Laboratory

prepared for
U.S. Department of Energy, National Nuclear Security Administration,
Office of Defense Nuclear Nonproliferation

September 30, 2008

CONTENTS

1 ABSTRACT 1

2 SUMMARY OF RESULTS 2

3 SCOPE 5

4 APPROACH/METHODS 6

4.1 Summary of Models Discussed in this Report 6
4.2 Chemical System of Interest 6
4.3 Process Used to Add Molybdenum Species to the GWB Database 7

5 RESULTS 10

5.1 Equilibration Models 10
5.2 Equilibrium Redox Speciation 10
5.3 Changes in Reactor Solution pH 12
5.4 Saturation State and Molybdenum Speciation 16
5.5 Precipitation of Uranyl Peroxide 18

6 CONCLUSIONS 20

7 FUTURE WORK 21

8 ACKNOWLEDGEMENTS 22

9 REFERENCES 23

FIGURES

1 Eh vs. pH Diagrams for Molybdenum, Uranium, and Iodine 15

2 Increase in pH of Reactor Solution due to Nitrogen Loss to Off-Gas and Iron Dissolution to Form Ferric Nitrate 16

3 Speciation of Reactor Solution as a Function of pH. 17

4 Left: Stability of the Uranyl Peroxide Mineral Studtite in Terms of the Concentration of Hydrogen Peroxide and pH; Right: Saturation Index for Uranyl Peroxide and Uranyl Oxide Hydrate vs. pH for 10^{-3} and 10^{-6} molar H_2O_2 for the Reactor Solution shown in Table 1. 19

TABLES

1 Molar Concentrations of Elements in the Model Reactor Solution Immediately after Being Discharged from the Reactor and after a 48-hour Cooling Period 3

2 Gibbs Free Energy of Formation Data Used to Calculate the Equilibrium Constants Needed to Add These Molybdenum Species to the GWB Thermodynamic Database 4

3 Gibbs Free Energy of Reaction and Equilibrium Constants for the Basis Reactions for Relevant Molybdenum Species 8

4 Constants for Redox Reactions Used in the GWB Database..... 8

5 Equilibrium Speciation of Reactor Solution at 25°C..... 11

6 Equilibrium Speciation of Reactor Solution at 80°C..... 13

REPORT DOCUMENTING THE SPECIATION OF METALS IN HOMOGENEOUS REACTOR SOLUTIONS: RERTR MILESTONE REPORT SEPTEMBER 30, 2008

1 ABSTRACT

Thermodynamic models of the solution chemistry in a homogeneous reactor used for molybdenum-99 (^{99}Mo) production are being developed at Argonne National Laboratory (Argonne) to aid in the optimization of molybdenum generation and recovery processes. The models calculate concentrations of aqueous species and saturation states of possible uranium and fission product precipitates (e.g., uranyl oxide hydrates, peroxides, molybdates) over a relevant range of pH values, oxidization/reduction potentials, and component concentrations. Predicting conditions under which precipitation may occur is particularly important because solids formed in the reactor solution could complicate ^{99}Mo recovery and have deleterious effects on reactor operation. Results presented in this paper indicate that, for uranyl nitrate based reactors, the radiolytic decomposition of nitrate (loss of nitrogen to off-gas) could cause the precipitation of uranyl and/or fission products due to an increase in pH. This precipitation process is readily counteracted by the addition of nitric acid. The modeling results presented help quantify the optimal pH envelope for a uranyl nitrate solution reactor used for ^{99}Mo production and highlight the need for future experimental studies to address uncertainties in the thermodynamic models.

2 SUMMARY OF RESULTS

The thermodynamic modeling presented in this paper has identified four processes that could adversely affect ^{99}Mo production from a uranyl nitrate solution reactor:

1. Fission product anions such as TcO_4^-, IO_3^-, I^-, Br^-, $HSeO_4^-$ and SeO_4^{2-}, which accumulate during burn-up (Tables 1 and 2), may compete with $HMoO_4^-$ or MoO_4^{2-} on anion exchange resins and might lower the molybdenum separation efficiency and influence product purity.

2. The loss of nitrate from the solution due to radiolysis and the corrosion of iron-bearing vessel components are expected to cause the pH of the reactor solution to increase to a value at which the solution is saturated with respect to uranium and molybdenum solids.

3. The reactor solution could become saturated with respect to uranyl molybdate and/or zirconium molybdate at pH values as low as 1. However, experimental studies are needed before the significance of uranyl or zirconium molybdate precipitation can be fully quantified.

4. If the steady-state concentration of hydrogen peroxide in the reactor reaches values near 1×10^{-3} molar, the uranyl peroxide solid studtite ($UO_2O_2{:}4H_2O$) could precipitate at pH values less than 1. However, if the steady-state concentration of hydrogen peroxide is 1×10^{-6} molar or lower, then the solution is predicted to become saturated with respect to uranyl peroxide at a pH value around 2.

These results provide a sound thermodynamic basis for prioritizing future experimental work to aid in the optimization of using a homogeneous aqueous reactor to produce Mo-99. Fugure experiments will be designed to account for kinetic and thermal effects. Some of the specific targets for experimental investigation include the following:

- Quantify the solubility constants for uranyl and zirconium molybdates.

- Quantify the stability constants of zirconium molybdate species.

- Quantify the steady-state concentration of hydrogen peroxide during reactor operation.

- Quantify the effects of radiolysis on the oxidation/reduction potential (Eh of the reactor solution.

TABLE 1 Molar Concentrations of Elements in the Model Reactor Solution Immediately after Being Discharged from the Reactor and after a 48-hour Cooling Period (The molybdenum concentration was fixed to reflect its being removed from the system regularly [on the order of days].)

Element[a]	After Discharge	After 48 Hours of Cooling
Uranium	1.0	1.0
Zirconium	5.4×10^{-4}	5.4×10^{-4}
Molybdenum	1.0×10^{-5}	1.0×10^{-5}
Cesium	3.5×10^{-4}	3.5×10^{-4}
Neodymium	3.1×10^{-4}	3.1×10^{-4}
Cerium	3.0×10^{-4}	3.0×10^{-4}
Ruthenium	2.2×10^{-4}	2.2×10^{-4}
Strontium	1.9×10^{-4}	1.9×10^{-4}
Plutonium	1.7×10^{-4}	1.7×10^{-4}
Barium	1.3×10^{-4}	1.3×10^{-4}
Lanthanum	1.2×10^{-4}	1.2×10^{-4}
Technetium	1.2×10^{-4}	1.2×10^{-4}
Praseodymium	9.9×10^{-5}	9.9×10^{-5}
Yttrium	9.7×10^{-5}	9.7×10^{-5}
Rubidium	6.5×10^{-5}	6.5×10^{-5}
Rhodium	4.7×10^{-5}	4.8×10^{-5}
Tellurium	4.1×10^{-5}	4.0×10^{-5}
Samarium	3.9×10^{-5}	3.9×10^{-5}
Promethium	3.5×10^{-5}	3.5×10^{-5}
Palladium	2.6×10^{-5}	2.6×10^{-5}
Iodine	1.8×10^{-5}	1.7×10^{-5}
Niobium	1.6×10^{-5}	1.6×10^{-5}
Selenium	9.8×10^{-6}	9.8×10^{-6}
Boron	8.8×10^{-6}	8.8×10^{-6}
Europium	3.6×10^{-6}	3.6×10^{-6}
Bromine	3.6×10^{-6}	3.6×10^{-6}
Neptunium	3.1×10^{-6}	2.2×10^{-6}
Tin	2.5×10^{-6}	2.5×10^{-6}
Cadmium	1.6×10^{-6}	1.6×10^{-6}
Antimony	1.1×10^{-6}	1.0×10^{-6}

[a] Only elements with concentrations $\geq 1 \times 10^{-6}$ molar were modeled.

TABLE 2 Gibbs Free Energy of Formation Data Used to Calculate the Equilibrium Constants Needed to Add These Molybdenum Species to the GWB Thermodynamic Database

Species	Phase	ΔG^o_f (kJ/mole)	Source
Mo	Metal	0	Bard et al. 1985
MoO_4^{2-}	Aqueous	–838.50	Bard et al. 1985
Mo^{3+}	Aqueous	–57.74	Faure 1998
MoO_2^{+}	Aqueous	–485.71	Bard et al. 1985[a]
MoO_2^{2+}	Aqueous	–413.59	Lindsay 1979[b]
$HMoO_4^{-}$	Aqueous	–893.70	Bard et al. 1985
H_2MoO_4	Aqueous	–882.80	Bard et al. 1985
$Mo_7O_{24}^{6-}$	Aqueous	–5251.00	Bard et al. 1985
$ZrMoO_4^{2+}$	Aqueous	–519.92	estimated
MoO_2	Crystalline	–533.01	Bard et al. 1985
MoO_3	Crystalline	–667.97	Bard et al. 1985
Mo_3O_8	Crystalline	–2008.32	Faure 1998
Mo_4O_{11}	Crystalline	–2512.00	Bard et al. 1985
H_2MoO_4	Crystalline	–912.00	Bard et al. 1985
UO_2MoO_4	Crystalline	unknown	model variable
$Zr(MoO_4)_2$	Crystalline	unknown	model variable
Rb_2MoO_4	Crystalline	–1387.00	Bard et al. 1985
Cs_2MoO_4	Crystalline	–1407.10	Bard et al. 1985
$Cs_2Mo_2O_7$	Crystalline	–2122.10	Bard et al. 1985
$SrMoO_4$	Crystalline	–1435.00	Bard et al. 1985
$BaMoO_4$	Crystalline	–1439.00	Bard et al. 1985
MoI_2	Crystalline	–110.50	Bard et al. 1985
MoI_3	Crystalline	–114.20	Bard et al. 1985
MoI_4	Crystalline	–77.40	Bard et al. 1985
MoI_5	Crystalline	–78.20	Bard et al. 1985
Auxiliary Species			
H^+	Aqueous	0	Faure 1998
H_2O	Aqueous	–237.14	Faure 1998
O_2	Aqueous	16.54	Faure 1998
Zr^{4+}	Aqueous	–594.13	Faure 1998
I^-	Aqueous	–51.92	Faure 1998
Rb^+	Aqueous	–284.01	Faure 1998
Cs^+	Aqueous	–291.46	Faure 1998
Sr^{2+}	Aqueous	–563.86	Faure 1998
Ba^{2+}	Aqueous	–557.66	Faure 1998

[a] Back calculated from E^o.

[b] Back calculated from $\log K_{eq}$.

3 SCOPE

Based on Babcock & Wilcox calculations for solution reactor fuel compositions, Argonne will look at potential chemical solubility concerns caused by hydrolysis as pH increases due to nitrate radiolysis. If the pH of the solution rises higher than expected values, hydrolysis of many metal ions (including U[VI]) can limit their solubilities. Calculations based on OLI Systems Inc. Environmental Simulation Program (ESP) and other codes will be used to develop a safe-pH operational envelope.

4 APPROACH/METHODS

4.1 SUMMARY OF MODELS DISCUSSED IN THIS REPORT

Thermodynamic models were implemented using the codes OLI ESP Stream Analyzer (OLI-SA) and "The Geochemist's Workbench®" Release 3.0 (GWB). The thermodynamic databases used for the OLI-SA modeling were the Geochemical, Corrosion, and Public databases that came with the software. The thermodynamic database used for modeling with GWB was an adapted version of the database thermo.com.V8.R6.full (Wolery and Daveler 1992). This database did not include molybdenum species, so these data were compiled from literature sources and incorporated into this database (see Section 2.3). In general, both modeling codes use a Gibb's free energy minimization technique to determine the equilibrium state of the system of interest. More specifically, the codes use the equilibrium constants for a set of basis reactions to solve a matrix of mass and charge balance equations. Results from these calculations feed into an iterative algorithm that converges on a unique equilibrium state for the multi-component, multi-phase system of interest. Kinetic effects can be incorporated in to models run using OLI-SA and GWB; however, as discussed below, this was not done for the simulations discussed in this report.

All of the models discussed in this report are equilibrium-based calculations; that is, no kinetic effects were accounted for. None of the species that may be produced by the radiolysis of water or nitrate are accounted for in the models discussed in this report, except for hydrogen peroxide (Section 5.5). The results from this work, therefore, represent an equilibrium baseline onto which kinetic effects can be superimposed. This equilibrium "context" may be used to account for the extent to which certain reactions deviate from equilibrium. A future focus of these modeling efforts will be to incorporate key kinetic effects into the reactor solution simulations.

4.2 CHEMICAL SYSTEM OF INTEREST

The composition of the reactor solution used for the models discussed in this report was calculated from a Microsoft Excel spreadsheet sent by e-mail to George Vandergrift from Gary Neeley of Babcock & Wilcox (Neely 2008). The spreadsheet gives the "light elements, actinides, and fission products in grams, for 90 day, 180 day, 270 day, and 365 day periods where the reactor is operated at 200 kW for 5 days, and the fission products are allowed to decay for two days, then the reactor is turned back on at 200 kW for 5 days etc."

The molar concentrations used for the simulations discussed in this report were calculated by first converting the grams of each isotope to moles; second, summing the moles of isotopes for a given element; and third, dividing the moles of a given element by the reactor solution volume in liters. The reactor solution volume used was 127.5 L (Beazley 2008).

For the models presented in this report we used concentrations derived from the 365-day period. The system used in the thermodynamic calculations was defined as a 1-M uranyl nitrate

solution containing 0.1-M nitric acid and the elements shown in Table 1 (concentrations were from the column labeled "After Discharge").

4.3 PROCESS USED TO ADD MOLYBDENUM SPECIES TO THE GWB DATABASE

The incorporation of the molybdenum data into the database required four steps: (1) Tabulating the free energies of formation (G^o_f) for species of interest, as well as auxiliary species that are used to write the basis reactions (Table 2). (2) Writing the basis reactions (Table 3). These reactions are used by the code to solve a matrix of mass and charge balance equations, which feed into an iterative algorithm that converges on a unique equilibrium state for the multi-phase, multi-component system of interest. (3) Calculating the free energy of reaction for the basis reactions (ΔG^o_r) using the following equation:

$$\Delta G_r^o = \sum_i n_i G_{fi}^o(\text{products}) - \sum_i n_i G_{fi}^o(\text{reactants}), \tag{1}$$

where n_i is the molar coefficient of species i in the reaction. (4) Calculating the equilibrium constants (K_{eq}) for the basis reactions using the following relationships:

$$\Delta G_r^o = -RT \ln K_{eq}. \tag{2}$$

The codes use $\log_{10}K_{eq}$ in their algorithms so the equation actually used is:

$$\log_{10} K_{eq} = -\frac{\Delta G_r^o}{2.303RT}, \tag{3}$$

where $K_{eq} = [A]^a[B]^b/[C]^c[D]^d$ for the reaction aA +bB + ↔ cC + dD; R is the gas constant; and T is absolute temperature.

The redox reactions used in the GWB database are shown in Table 4. The equilibrium redox speciation is presented below in terms of Eh, which is defined as the electromotive force (emf) generated between an electrode in any state and the hydrogen electrode [$H_2(g) \rightarrow 2H^+ + 2e^-$] in the standard state. The hydrogen electrode in the standard state has a standard potential or standard emf (E^o) of zero. The emf is the electrical potential generated by a redox half-reaction. Eh is calculated using the following relationships (for the half reaction aA +bB + ne^- + ↔ cC + dD):

$$Eh = E^o + \frac{RT}{nF} \ln \frac{(A)^a (B)^b}{(C)^c (D)^d}, \tag{4}$$

TABLE 3 Gibbs Free Energy of Reaction and Equilibrium Constants for the Basis Reactions for Relevant Molybdenum Species (calculated using Gibbs free energy data shown in Table 2 and equations [1]–[3])

Basis Reactions	ΔG^o_r (kJ/mole)	$\log_{10}K$
$MoO_2^{2+} + 2H_2O \leftrightarrow MoO_4^{2-} + 4H^+$	49.37	–8.65
$HMoO_4^- \leftrightarrow MoO_4^{2-} + H^+$	55.20	–9.67
$H_2MoO_4(aq) \leftrightarrow MoO_4^{2-} + 2H^+$	44.30	–7.76
$Mo_7O_{24}^{6-} + 4H_2O \leftrightarrow 7MoO_4^{2-} + 8H^+$	330.06	–57.81
$MoO_2(c) + 0.5O2(aq) + H_2O \leftrightarrow MoO_4^{2-} + 2H^+$	–76.62	13.42
$MoO_3(c) + H_2O \leftrightarrow MoO_4^{2-} + 2H^+$	99.70	–17.46
$Mo_3O_8(c) \leftrightarrow MoO_4^{2-} + 2MoO2+$	142.23	–24.91
$Mo_4O_{11}(c) + H2O \leftrightarrow 2MoO_4^{2-} + 2MoO2+ + 2H^+$	44.55	–7.80
$H_2MoO_4(c) \leftrightarrow MoO_4^{2-} + 2H^+$	73.50	–12.87
$Rb_2MoO_4(c) \leftrightarrow MoO_4^{2-} + 2Rb^+$	–19.52	3.42
$Cs_2MoO_4(c) \leftrightarrow MoO_4^{2-} + 2Cs^+$	–14.31	2.51
$Cs_2Mo_2O_7(c) + H_2O \leftrightarrow MoO_4^{2-} + 2Cs^+ + 2H^+$	99.33	–17.40
$SrMoO_4(c) \leftrightarrow MoO_4^{2-} + Sr^{2+}$	32.636	–5.72
$BaMoO_4(c) \leftrightarrow MoO_4^{2-} + Ba^{2+}$	42.844	–7.50
$MoI_2(c) + O_2(aq) + 2H_2O \leftrightarrow MoO_4^{2-} + 2I^- + 4H^+$	–374.11	65.53
$MoI_3(c) + 0.75O_2(aq) + 2.5H_2O \leftrightarrow MoO_4^{2-} + 3I^- + 5\ H^+$	–528.03	92.49
$MoI_4(c) + 0.5O_2(aq) + 3H_2O \leftrightarrow MoO_4^{2-} + 4I^- + 6H^+$	–265.65	46.53
$MoI_5(c) + 0.25O_2(aq) + 3.5H_2O \leftrightarrow MoO_4^{2-} + 5I^- + 7H^+$	–194.06	33.99

TABLE 4 Constants for Redox Reactions Used in the GWB Database (These constants were calculated using equations [1]–[7] and the Gibbs free energy of formation data shown in Table 2.)

Redox Reaction	Redox Transition	E^o	ΔG^o_r (kJ/mole)	$\log_{10}K$
$MoO_2^{2+} + e^- \rightarrow MoO_2^+$	Mo(VI)/Mo(V)	0.77	–74.61	13.07
$MoO_2^{2+} + 4H^+ + 3e^- \rightarrow Mo^{3+} + 2H_2O$	Mo(VI)/Mo(III)	0.41	–118.53	20.76
$MoO_3 + 2H^+ + e^- \rightarrow H_2O + MoO_2^+$	Mo(VI)/Mo(V)	0.37	–35.51	6.22
$MoO_3 + 6H^+ + 3e^- \rightarrow Mo+++ + 3H2O$	Mo(VI)/Mo(III)	0.26	–75.20	13.17
$HMoO_4^- + 3H^+ + e^- \rightarrow MoO_2^+ + 2H_2O$	Mo(VI)/Mo(V)	0.71	–68.79	12.05
$HMoO_4^- + 3H^+ + e^- \rightarrow MoO_2^+ + 2H_2O$	Mo(VI)/Mo(V)	0.40	–77.19	13.52
$HMoO_4^- + 3H^+ + 2e^- \rightarrow MoO_2 + 2H_2O$	Mo(VI)/Mo(IV)	0.59	–113.65	19.91
$H_2MoO_4(aq) + 2H^+ + e^- \rightarrow MoO_2^+ + 2H_2O$	Mo(VI)/Mo(V)	0.83	–79.69	13.96
$H_2MoO_4(aq) + 2H^+ + 2e^- \rightarrow MoO_2 + 2H_2O$	Mo(VI)/Mo(IV)	0.65	–124.55	21.82
$H_2MoO_4(aq) + 3e^- + 6H^+ \rightarrow Mo^{3+} + 4H_2O$	Mo(VI)/Mo(III)	0.43	–123.61	21.66
$MoO_4^{2-} + 2e^- + 4H^+ \rightarrow MoO_2 + 2H_2O$	Mo(VI)/Mo(IV)	0.87	–168.85	29.58
$MoO_2^+ + 2e^- + 4H^+ \rightarrow 2H_2O + Mo^{3+}$	Mo(VI)/Mo(III)	0.23	–43.92	7.69
$MoO_2^+ + e- \rightarrow MoO_2$	Mo(VI)/Mo(IV)	0.46	–44.86	7.86
$MoO_2^+ + 4H^+ + 5e^- \rightarrow Mo + 4H_2O$	Mo(V)/Mo(0)	–0.02	11.63	–2.04
$MoO_2 + 4H^+ + e^- \rightarrow Mo^{3+} + 2H_2O$	Mo(IV)/Mo(III)	–0.01	0.95	–0.17

which is equivalent to

$$Eh = E^o + 2.303\frac{RT}{nF}\log_{10} K_{eq}, \tag{5}$$

where n is the number of electrons transferred during the half-reaction and F is the Faraday constant. The standard potential (E^o) is related to the change in the Gibbs free energy of formation and $\log_{10}K_{eq}$ for the half-reaction as follows:

$$E^o = \frac{\Delta G_r^o}{nF}, \tag{6}$$

and therefore,

$$E^o = -\frac{2.303RT}{nF}\log_{10} K_{eq}. \tag{7}$$

The solution saturation state is presented in terms of the saturation index (SI), which is defined as follows:

$$SI = \log_{10}\frac{Q}{K_{sp}}, \tag{8}$$

where Q is the reaction quotient defined as $Q = [A]^a[B]^b/[A_aB_b]$ for the reaction $aA + bB + \leftrightarrow A_aB_b$, and K_{sp} is the equilibrium constant for the precipitation/dissolution reaction in question. The reaction quotient changes continuously during the reaction until equilibrium is achieved and is related to the change in the Gibbs free energy of reaction as follows:

$$\Delta G_r = \Delta G_r^o + RT\ln Q, \tag{9}$$

and therefore,

$$\log_{10} Q = \frac{\Delta G_r - \Delta G_r^o}{2.303RT}. \tag{10}$$

At equilibrium ΔG_r goes to zero and therefore $Q = K_{sp}$:

$$\log_{10} K_{sp} = -\frac{\Delta G_r^o}{2.303RT}. \tag{11}$$

Therefore, at equilibrium, SI = 0; if the reaction is written with the solid phase as a reactant, if SI < 0, the solution is undersaturated with respect to that mineral, and if SI = 0, the solution is saturated.

5 RESULTS

5.1 EQUILIBRATION MODELS

Equilibrium speciation of the reactor solution was calculated using OLI SA at 25°C and 80°C (results shown in Tables 5 and 6). The reactor solution is 1-M uranyl nitrate with 0.1-M nitric acid, and concentrations of fission and activation products are shown in Table 1. At 25°C, the equilibrium pH, oxidation/reduction potential (Eh) and density are predicted to be 1.18, 1.1 volts, and 1.3 g/mL, respectively. At 80°C the pH, Eh and density are predicted to be 1.24, 1.11 volts, and 1.28 g/mL, respectively. At 25°C, the solution is saturated with respect to tin oxide (SnO_2). Some of the key cationic species for both the 25°C and 80°C case include the uranyl ion, uranyl hydroxide, zirconium hydroxide, lanthanide nitrates, plutonyl(VI) nitrate, plutonyl(VI), neptunyl(V), uranyl iodate, and zirconium molybdate. It should be noted that uranyl nitrate (UO_2NO3^+) is not included in the OLI databases; however, the GWB models, discussed below, predict that uranyl nitrate is an important cationic species. The main neutral species for both temperature runs include cesium and strontium nitrates, as well as plutonyl(VI) dinitrate. The dominant anions for both temperature runs include nitrate, pertechnetate, selenate, hydrogen selenate, hydrogen molybdate, bromide, and iodate (for more details see Tables 5 and 6).

The relatively high concentration of zirconium molybdate for the 25°C case is of specific interest because it implies that, at a pH of 1.18, around half of the molybdenum is present in a cationic state. This could potentially lower molybdenum recovery by anion exchange. However, the stability constant for the zirconium molybdate complex appears to be uncertain, because it is not included in many of the standard thermodynamic compilations for molybdenum (e.g., Bard et al. 1985; Martell et al. 2004). This uncertainty should be considered a key target for future work.

5.2 EQUILIBRIUM REDOX SPECIATION

To establish a general context for how changes in redox conditions and hydrogen ion activity could influence the speciation of the reactor solution, Eh versus pH diagrams were plotted for the system of interest. Examples for some of the key elements (i.e., uranium, molybdenum, and iodine) are shown in Figure 1. These diagrams, which show the predicted equilibrium Eh–pH conditions for the reactor solution as yellow circles, indicate that the uranyl ion, uranyl nitrate, hydrogen molybdate, iodate, and uranyl iodate are predicted to be dominant species. They also imply that if the Eh of the solution decreases, perhaps due to radiolysis or hydrogen production, the speciation of molybdenum and iodine could be significantly affected. For example, hydrogen molybdate could be reduced to MoO_2^+ and iodate could be reduced to I_2 or iodide.

TABLE 5 Equilibrium Speciation of Reactor Solution at 25°C[a]

Aqueous	Molar	mg/kg
NO_3^-	2.1	$9.4 \times 10^{+4}$
UO_2^{2+}	1.0	$1.9 \times 10^{+5}$
H^+	9.4×10^{-2}	67.7
$ZrOH^{3+}$	4.5×10^{-4}	35.1
$NdNO_3^{2+}$	2.3×10^{-4}	33.7
$CeNO_3^{2+}$	2.2×10^{-4}	32.5
Ru^{3+}	2.2×10^{-4}	16.0
$CsNO_3$	2.1×10^{-4}	29.7
Cs^+	1.4×10^{-4}	13.2
Ba^{2+}	1.3×10^{-4}	12.8
TcO_4^-	1.2×10^{-4}	14.1
La^{3+}	1.1×10^{-4}	11.1
$(UO_2)_2(OH)_2^{2+}$	1.0×10^{-4}	43.2
$Sr(NO_3)_2$	9.0×10^{-5}	13.8
Nd^{3+}	8.2×10^{-5}	8.6
Zr^{4+}	8.2×10^{-5}	5.4
Ce^{3+}	7.6×10^{-5}	7.7
$PrNO_3^{2+}$	6.6×10^{-5}	9.6
$Y(NO_3)_2^+$	6.5×10^{-5}	9.9
Rb^+	6.5×10^{-5}	4.0
$PuO_2(NO_3)_2$	6.3×10^{-5}	18.1
$PuO_2NO_3^+$	6.1×10^{-5}	14.7
$SrNO_3^+$	5.6×10^{-5}	6.4
Rh^{3+}	4.7×10^{-5}	3.4
Sr^{2+}	4.3×10^{-5}	2.7
$Te(OH)_3^+$	4.1×10^{-5}	5.3
PuO_2^{2+}	3.0×10^{-5}	6.0
Pr^{3+}	3.3×10^{-5}	3.4
UO_2OH^+	3.2×10^{-5}	6.7
Sm^{3+}	3.0×10^{-5}	3.2
YNO_3^{2+}	2.9×10^{-5}	3.2
Pd^{2+}	2.1×10^{-5}	1.6
$UO_2IO_3^+$	9.0×10^{-6}	2.9
$SmNO_3^{2+}$	8.9×10^{-6}	1.4
$Pu(NO_3)_4$	8.9×10^{-6}	3.2
$B(OH)_3$	8.8×10^{-6}	0.39
$LaNO_3^{2+}$	8.6×10^{-6}	1.3
$ZrMoO_4^{2+}$	6.8×10^{-6}	1.2
SeO_4^{2-}	6.3×10^{-6}	0.65
$Pu(NO_3)_3^+$	5.8×10^{-6}	1.8
I_2	4.0×10^{-6}	0.7
Br^-	3.5×10^{-6}	0.20
$HSeO_4^-$	3.5×10^{-6}	0.4
$HMoO_4^-$	3.2×10^{-6}	0.36
Y^{3+}	3.2×10^{-6}	0.21
$PdOH^+$	3.2×10^{-6}	0.28

TABLE 5 (Cont.)

Aqueous	Molar	mg/kg
NpO_2^+	2.9×10^{-6}	0.57
$EuNO_3^{2+}$	2.8×10^{-6}	0.43
HNO_3	1.7×10^{-6}	0.08
Rh^{2+}	1.5×10^{-6}	1.1
$Pu(NO_3)_2^{2+}$	1.4×10^{-6}	0.36
$Pd(OH)_2$	1.4×10^{-6}	0.15
MoO_4^{2-}	1.2×10^{-6}	0.14
Cd^{2+}	9.1×10^{-7}	0.07
Eu^{3+}	8.5×10^{-7}	0.09
$CdNO_3^+$	6.9×10^{-7}	0.09
IO_3^-	3.4×10^{-7}	0.04
$Sb(OH)_5$	5.5×10^{-7}	0.08
HIO	5.1×10^{-7}	0.05
$RuOH^{2+}$	4.1×10^{-7}	0.04
H_3SbO_4	4.0×10^{-7}	0.05
$Zr(OH)_2^{2+}$	2.7×10^{-7}	0.02
PuO^{2+}	2.1×10^{-7}	0.04
HIO_3	1.5×10^{-7}	0.02
$Sn(OH)_4$	1.0×10^{-7}	0.01

[a] Starting concentrations are from Table 1. Aqueous properties: temperature = 25°C; pH = 1.18; (H^+) activity coefficient = 0.699; Eh= 1.07 volts; and density = 1.33 g/mL. Saturation index (in $\log_{10}Q/K$): SnO_2 = 0; ZrO_2 = –1.74.

5.3 CHANGES IN REACTOR SOLUTION pH

The GWB code was used to simulate the change in speciation and saturation state of the reactor solution with increasing pH. Processes that could drive the solution pH to higher values during reactor operation include the radiolytic destruction of nitrate and subsequent loss of nitrogen as a gaseous species, as well as the corrosion of steel walls of the reactor vessel and components. For both processes, the pH increases steadily as either nitrogen is “titrated” out of the system or iron is titrated into the system. These processes can be summarized by the following general reactions:

$$NO_3^- + H^+ \rightarrow 0.5H_2O + 0.5N_2(g) + 1.25O_2(aq) \qquad \text{(Reaction 1)}$$

$$Fe + 3H^+ + 0.75O_2(aq) + NO_3^- \rightarrow FeNO_3^{2+} + 1.5H_2O \qquad \text{(Reaction 2)}$$

The increase in pH is countered by hydrolyses of the uranyl and ferric ions (reactions 3 and 4) as well as by the precipitation of ferric hydroxides or oxides (reactions 5 and 6), uranyl

TABLE 6 Equilibrium Speciation of Reactor Solution at 80°C[a]

Aqueous	Molar	mg/kg
NO_3^-	2.1	$9.4 \times 10^{+4}$
UO_2^{2+}	1.0	$1.9 \times 10^{+5}$
H^+	9.8×10^{-2}	70.7
$(UO_2)_2(OH)_2^{2+}$	1.6×10^{-3}	675.5
UO_2OH^+	6.8×10^{-4}	140.5
$ZrOH^{3+}$	3.6×10^{-4}	28.3
$CsNO_3$	2.4×10^{-4}	33.4
Ru^{3+}	2.1×10^{-4}	15.6
Nd^{3+}	2.0×10^{-4}	20.2
$CeNO_3^{2+}$	1.9×10^{-4}	27.2
Ba^{2+}	1.3×10^{-4}	12.8
$Sr(NO_3)_2$	1.3×10^{-4}	19.1
TcO_4^-	1.2×10^{-4}	14.1
La^{3+}	1.2×10^{-4}	11.7
$NdNO_3^{2+}$	1.1×10^{-4}	17.0
Ce^{3+}	1.1×10^{-4}	11.4
Cs^+	1.1×10^{-4}	10.7
HNO_3	7.1×10^{-5}	3.2
Pr^{3+}	6.8×10^{-5}	6.9
$Zr(OH)_3^+$	6.7×10^{-5}	6.8
Rb^+	6.5×10^{-5}	4.0
$Pu(NO_3)_4$	6.4×10^{-5}	22.8
PuO^{2+}	4.5×10^{-5}	9.0
$SrNO_3^+$	4.5×10^{-5}	4.9
Y^{3+}	4.5×10^{-5}	2.9
$PuO_2NO_3^+$	4.0×10^{-5}	9.7
$Te(OH)_3^+$	4.0×10^{-5}	5.1
Rh^{3+}	3.9×10^{-5}	2.9
$Y(NO_3)_2^+$	3.7×10^{-5}	4.0
Sm^{3+}	3.6×10^{-5}	3.9
$PrNO_3^{2+}$	3.1×10^{-5}	4.5
Pd^{2+}	2.0×10^{-5}	1.6
Sr^{2+}	1.9×10^{-5}	1.2
$PuO_2(NO_3)_2$	1.8×10^{-5}	5.2
$UO_2IO_3^+$	1.8×10^{-5}	5.6
YNO_3^{2+}	1.6×10^{-5}	2.4
$HMoO_4^-$	9.2×10^{-6}	1.1
$B(OH)_3$	8.8×10^{-6}	0.4
Rh^{2+}	7.0×10^{-6}	0.5
$HSeO_4^-$	6.1×10^{-6}	0.6
$RuOH^{2+}$	5.2×10^{-6}	0.4
Zr^{4+}	4.9×10^{-6}	0.3
$PdOH^+$	4.0×10^{-6}	0.4
SeO_4^{2-}	3.7×10^{-6}	0.4
Br^-	3.5×10^{-6}	0.2
NpO_2^+	2.9×10^{-6}	0.6

TABLE 6 (Cont.)

Aqueous	Molar	mg/kg
$SmNO_3^{2+}$	2.6×10^{-6}	0.4
$LaNO_3^{2+}$	2.5×10^{-6}	0.4
Eu^{3+}	2.3×10^{-6}	0.3
$Pd(OH)_2$	1.7×10^{-6}	0.2
$RhOH^{2+}$	1.7×10^{-6}	0.2
$Sb(OH)_4$	1.6×10^{-6}	0.2
H_2TeO_3	1.3×10^{-6}	0.2
$EuNO_3^{2+}$	1.3×10^{-6}	0.2
$Pu(NO_3)_3^{+}$	1.1×10^{-6}	0.35
H_3SbO_4	9.6×10^{-7}	0.1
$Zr(OH)_2^{2+}$	9.6×10^{-7}	0.09
Cd^{2+}	8.0×10^{-7}	0.06
$CdNO_3^{+}$	8.0×10^{-7}	0.1
$Zr(OH)_4$	7.9×10^{-7}	0.09
$ZrMoO_4^{2+}$	7.4×10^{-7}	1.3
$Ru(OH)_2^{+}$	7.3×10^{-7}	0.07
$Pu(NO_3)_2^{2+}$	5.6×10^{-7}	0.15
$Rh(OH)_2^{+}$	5.4×10^{-7}	0.05
PuO_2^{+}	5.2×10^{-7}	0.1
$SnOH^{3+}$	4.8×10^{-7}	0.05
Sn^{4+}	2.4×10^{-7}	0.02
IO_3^{-}	2.3×10^{-7}	0.03
HIO_3	2.1×10^{-7}	0.03
$SnOH_3^{+}$	1.2×10^{-7}	0.01

[a] Starting concentrations are from Table 1. Aqueous properties: temperature = 80°C; pH = 1.24; (H^+) activity coefficient = 0.590; Eh (for solids with SI > –3) = 1.11 volts; and density = 1.28 g/mL. Saturation index (in $\log_{10}Q/K$): ZrO_2 = 0; SnO_2 = –0.04.

oxide hydrate (reaction 7), and possibly uranyl peroxide (reaction 8); if the steady state concentration of radiolytic hydrogen peroxide is high enough ("s" indicates solid):

$$2UO_2^{2+} + 2H_2O \leftrightarrow (UO_2)_2(OH)_2^{2+} + 2H^+ \qquad \text{(Reaction 3)}$$

$$2H_2O + 2FeNO_3^{2+} \leftrightarrow Fe_2(OH)_2^{4+} + 2NO_3^- + 2H^+ \qquad \text{(Reaction 4)}$$

$$FeNO_3^{2+} + 3H_2O \leftrightarrow Fe(OH)_3(s) + 3H^+ + NO_3^- \qquad \text{(Reaction 5)}$$

$$2FeNO_3^{2+} + 3H_2O \leftrightarrow Fe_2O_3(s) + 6H^+ + 2NO_3^- \qquad \text{(Reaction 6)}$$

$$UO_2^{2+} + 3H_2O \leftrightarrow UO_3{:}2H_2O(s) + 2H^+ \qquad \text{(Reaction 7)}$$

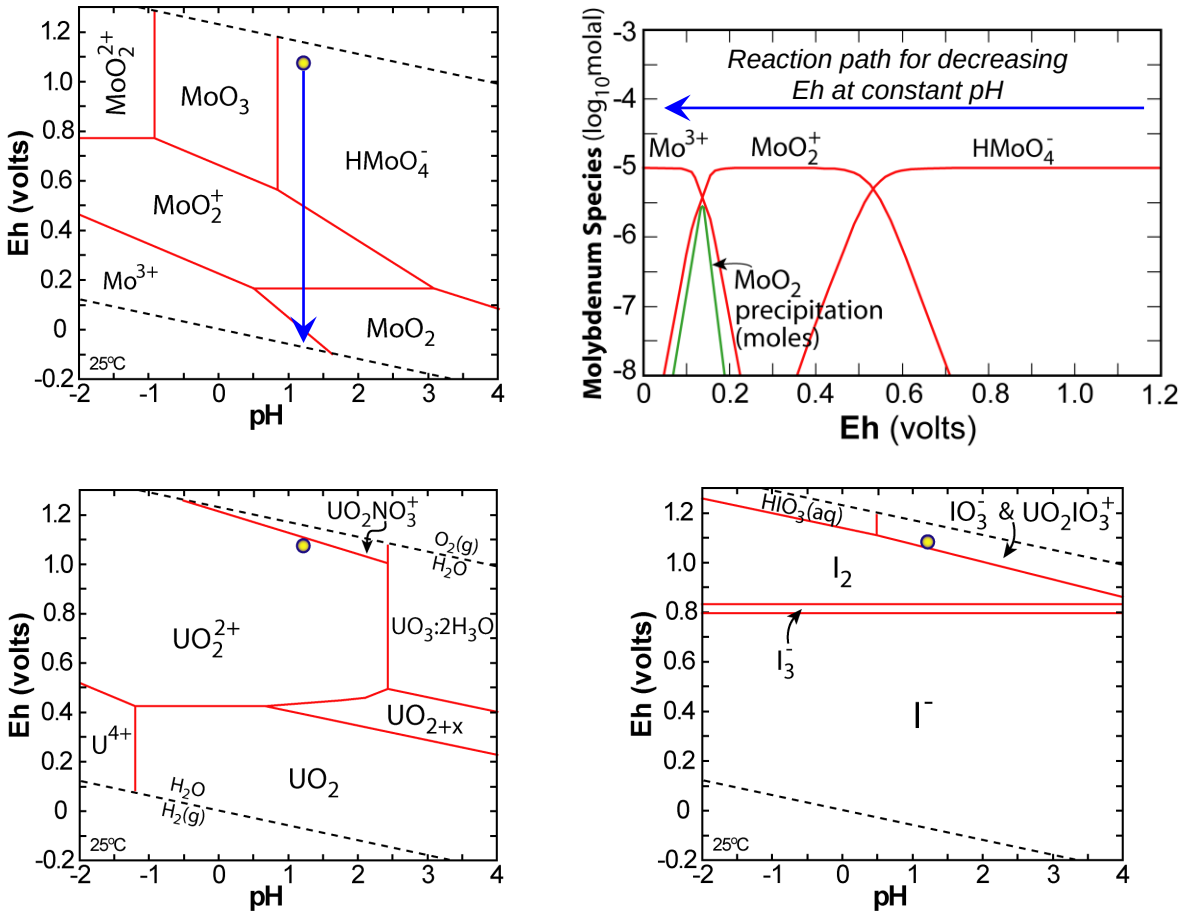

FIGURE 1 Eh vs. pH Diagrams for Molybdenum, Uranium, and Iodine (The conditions for the reactor solution are shown as a yellow dot [plots drawn for 25°C]. The blue line in the molybdenum diagram [upper left] shows a reaction path involving a decrease in Eh at constant pH [as could be caused by radiolysis or H_2 gas interacting with the solution]. The concentrations of the molybdenum species along this decreasing Eh reaction path are shown in the upper right hand diagram. The dotted black lines on all of the Eh vs. pH diagrams indicate the stability field of water [$H_2O \leftrightarrow O_2(g)$ and $H_2O \leftrightarrow H_2(g)$]. All plots are for concentrations shown in Table 1.)

$$UO_2^{2+} + 4H_2O + H_2O_2 \leftrightarrow UO_2O_2{:}4H_2O(s) + 2H^+ \qquad \text{(Reaction 8)}$$

Results from simulations of the pH increase that could be caused by reactions 1 and 2 are shown in Figure 1. The dotted lines in these plots show how the pH increase would be counteracted (buffered) by the precipitation of uranyl oxide hydrate and ferric hydroxide (reactions 5 and 7). These models predict that the pH of the reactor solution could increase to values as high as 3.0, depending on precipitation kinetics. Other speciation models were run for the reactor solution (Table 1) for a pH range extending from –2 (slightly lower than concentrated nitric acid) to 4 (a conservative high end of possible pH envelop for the reactor solution).

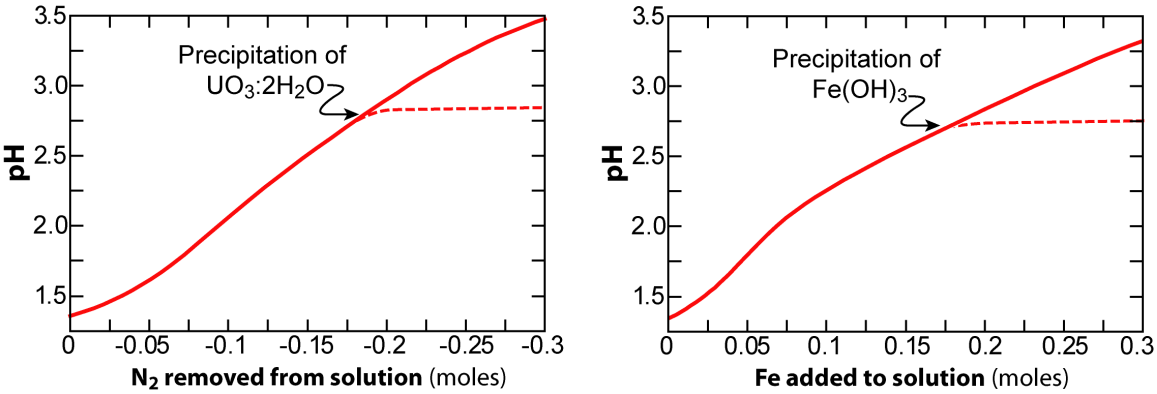

FIGURE 2 Increase in pH of Reactor Solution due to Nitrogen Loss to Off-Gas (left, solid line, reaction 1) and Iron Dissolution to Form Ferric Nitrate (right, solid line, reaction 2) (The pH increase is counteracted by precipitation reactions [dotted lines, reactions 5 and 7].)

5.4 SATURATION STATE AND MOLYBDENUM SPECIATION

Results showing the saturation state and speciation of molybdenum over the pH range –2 to 4 are shown in Figure 3. These plots highlight how the uncertainty in thermodynamic data can significantly affect the predicted speciation of the solution. For example, Figure 3a shows the saturation indices for the two key uranium solids. The model predicts that the reactor solution would become saturated with respect to uranyl oxide hydrate at a pH around 3; however, there is uncertainty as to the solubility product (K_{sp}) of uranyl molybdate. Sparse experimental data (e.g., Prasad and Barros 1998; Ferris 1961) suggest the $\log_{10}K_{sp}$ for uranyl molybdate falls in the range of –13 to –15 (for the basis reaction: $UO_2MoO_4(s) \leftrightarrow UO_2^{2+} + MoO_4^{2-}$). When the model is run using $\log_{10}K_{sp} = -15$, the reactor solution becomes saturated with uranyl molybdate at pH 1; however, if $\log_{10}K_{sp} = -13$, then uranyl molybdate is not predicted to precipitate in this system (Figure 3a) (remains slightly undersaturated).

Figure 3b shows the saturation indices for the two key molybdenum solids. The model predicts that the reactor solution would become saturated with respect to molybdenum oxide at a pH around –0.5; however, there is uncertainty as to the K_{sp} for zirconium molybdate. Some experimental data suggest that the $\log_{10}K_{sp}$ for uranyl molybdate fall in the range of –34 to –36 (for the basis reaction: $Zr(MoO_4)_2(s) \leftrightarrow Zr^{4+} + 2MoO_4^{2-}$). When the model is run using $\log_{10}K_{sp} = -36$, the reactor solution becomes saturated with zirconium molybdate at pH = 0.5; however, if $\log_{10}K_{sp} = -34$, then zirconium molybdate is not predicted to precipitate in this system (Figure 3b). Figure 3c shows molybdenum speciation for a case in which molybdenum oxide and uranyl molybdate precipitate. Molybdenyl(VI) is predicted to be the main species at low pH and its concentration drops from 1×10^{-5} molar down to $1 \times 10^{-6.5}$ molar due to the precipitation of molybdenum(VI) oxide. Above pH = 0, hydrogen molybdate becomes the dominant molybdenum species; however, zirconium molybdate is also predicted to be a significant species around pH 1 (concentration of zirconium molybdate is dotted to signify uncertainty in its stability constant). With the precipitation of uranyl molybdate, the hydrogen

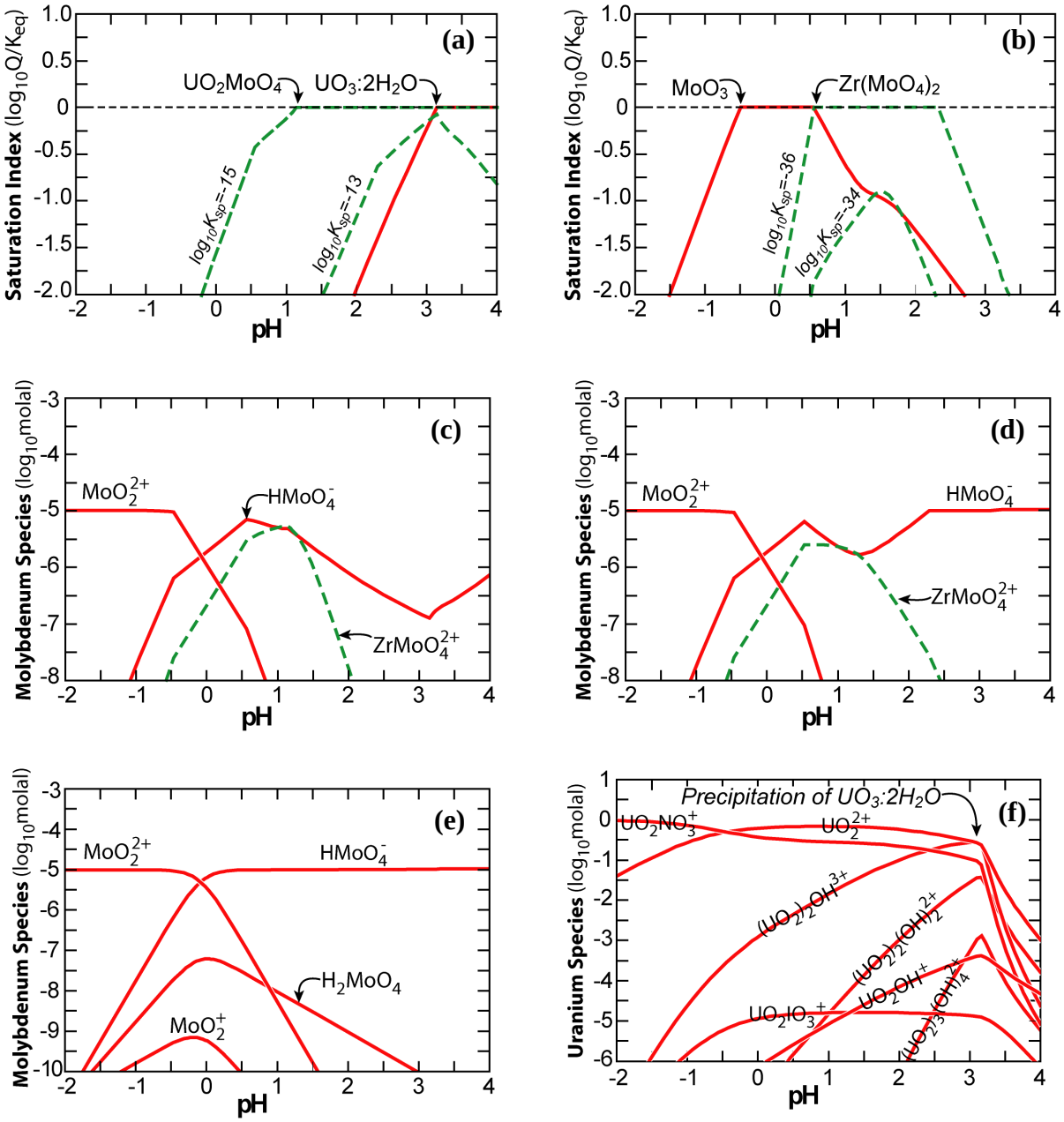

FIGURE 3 Speciation of Reactor Solution as a Function of pH (compositions from Table 1, Eh from Table 5). (a) Mineral saturation index plot for key uranium solids (see text above for discussion). (b) Mineral saturation index plot for key molybdenum solids. (c) Molybdenum speciation for the case where molybdenum oxide and uranyl molybdate precipitate. (d) Molybdenum speciation for the case where molybdenum oxide and zirconium molybdate precipitate. (e) Molybdenum speciation diagram for the case where no minerals precipitate. (f) Uranium speciation plot showing increased concentrations of uranyl hydroxide species with increasing pH, and the precipitation of uranyl oxide hydrate around pH = 3.

molybdate concentration decreases from a maximum of $1 \times 10^{-6.75}$ molar at pH = 0.5, to a minimum of around 1×10^{-7} molar around pH = 3. Figure 3d shows molybdenum speciation for a case in which molybdenum oxide and zirconium molybdate precipitate, but uranyl molybdate does not. Again, molybdenyl(VI) is predicted to be the main species at low pH and its concentration drops from 1×10^{-5} molar down to $1 \times 10^{-6.5}$ molar due to the precipitation of molybdenum(VI) oxide. Above pH = 0, hydrogen molybdate becomes the dominant molybdenum species; however, zirconium molybdate is also predicted to be a significant species around pH 1. Around pH 1.5, the concentration of hydrogen molybdate drops to a value of approximately 1×10^{-6} molar due to the precipitation of zirconium molybdate.

Figure 3e shows molybdenum speciation for a case in which none of the solids precipitate (perhaps due to kinetic inhibitions). This plot reiterates the dominance of molybdenyl(VI) at low pH and hydrogen molybdate above a pH value of zero. Figure 3f shows that uranium speciation is dominated by uranyl nitrate and the uranyl ion at low pH, and by uranyl hydroxides at higher pH.

Another potentially important precipitate is the uranyl peroxide solid studtite ($UO_2O_2{:}4H_2O$). Key thermodynamic properties of this mineral have been quantified (Kubatko et al. 2003); however, its importance in the reactor solution is unknown due to uncertainties in the steady-state concentration of hydrogen peroxide in the irradiated fuel during reactor operation. It is anticipated that hydrogen peroxide will be produced during reactor operation by radiolysis of water. Depending on the ratio of the rates of hydrogen peroxide formation and auto destruction, a steady-state concentration will be established. If this concentration is high enough, it could cause uranium to precipitate as the sparingly soluble uranyl peroxide studtite at a pH value less 3.0. The model results in Figure 4 establish the pH range over which uranyl peroxide precipitation may occur for a given steady-state concentration of hydrogen peroxide.

5.5 PRECIPITATION OF URANYL PEROXIDE

The plot on the left side of Figure 4 shows the stability of uranyl peroxide in terms of hydrogen peroxide molality and pH. The thermodynamic data used to assess the saturation index for uranyl peroxide (incorporated in to the GWB database) are from Kubatko et al. (2003). The model predicts that, at a hydrogen peroxide concentration as low as approximately 1×10^{-7} molar, uranyl peroxide may be stable at a pH around 2.5. At higher hydrogen peroxide concentrations the pH stability threshold decreases. For example, as shown in the plot on the right side of Figure 4, the reactor solution could become saturated with respect to uranyl peroxide at a pH as low as 0.5 if the steady state concentration of hydrogen peroxide is 1×10^{-3} molar or as high as pH = 2 if the concentration is 1×10^{-6} molar. More information about the rate of hydrogen peroxide production and auto destruction is needed to accurately predict the significance of uranyl peroxide precipitate during uranyl solution reactor operation.

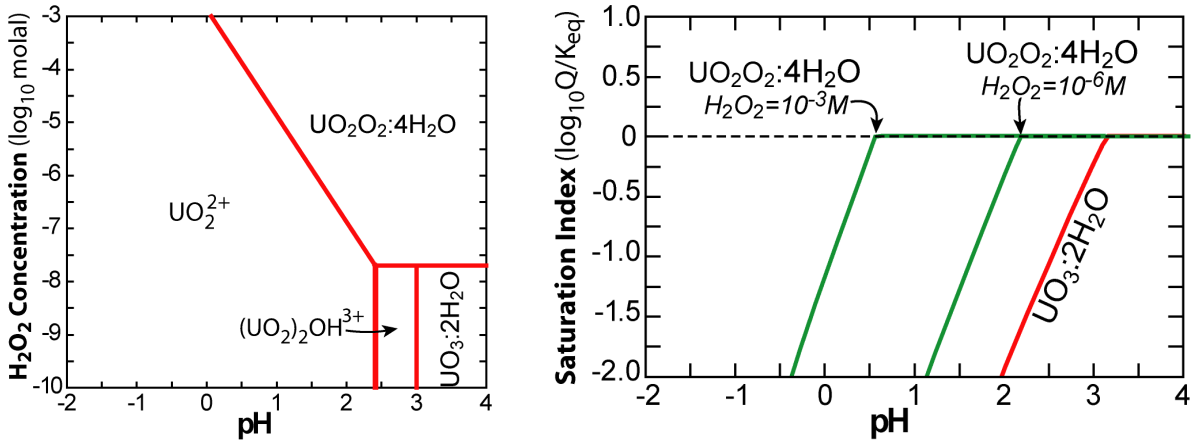

FIGURE 4 Left: Stability of the Uranyl Peroxide Mineral Studtite in Terms of the Concentration of Hydrogen Peroxide and pH; Right: Saturation Index for Uranyl Peroxide and Uranyl Oxide Hydrate vs. pH for 10^{-3} and 10^{-6} molar H_2O_2 for the Reactor Solution shown in Table 1.

6 CONCLUSIONS

The thermodynamic modeling presented in this paper has identified four processes that could adversely affect ^{99}Mo production from a uranyl nitrate solution reactor:

1. Fission product anions such as TcO_4^-, IO_3^-, I^-, Br^-, $HSeO_4^-$, and SeO_4^{2-}, which accumulate during burn-up, may compete with $HMoO_4^-$ or MoO_4^{2-} on anion exchange resins and might lower the molybdenum separation efficiency and influence product purity. If experiments show this phenomenon to be a significant issue, it can be counteracted by reprocessing the fuel solution at regular intervals to remove competing species.

2. The loss of nitrate from the solution due to radiolysis and the corrosion of iron bearing vessel components are expected to cause the pH of the reactor solution to increase to a value at which the solution is saturated with respect to uranium and molybdenum solids. Such an increase in pH could be counteracted by adding nitric acid to the solution to compensate for nitrogen loss and by using metals that are resistant to corrosion (e.g., zirconium-based alloys) for vessel component construction.

3. The reactor solution could become saturated with respect to uranyl molybdate and/or zirconium molybdate at pH values as low as 1. However, experimental studies are needed before the significance of uranyl or zirconium molybdate precipitation can be fully quantified.

4. If the steady-state concentration of hydrogen peroxide in the reactor reaches values near 1×10^{-3} molar, the uranyl peroxide solid studtite ($UO_2O_2{:}4H_2O$) could precipitate at pH values less than 1. However, if the steady-state concentration of hydrogen peroxide is 1×10^{-6} molar or lower, then the solution is predicted to become saturated with respect to uranyl peroxide at a pH value around 2. If experiments indicate that uranyl peroxide precipitation is an issue for reactor operation, the process could be counteracted by adding a material that catalyzes the auto destruction of hydrogen peroxide.

7 FUTURE WORK

These results provide a sound thermodynamic basis for prioritizing future experimental work to aid in the optimization of using a homogeneous aqueous reactor to produce Mo-99. Fugure experiments will be designed to account for kinetic and thermal effects. Some of the specific targets for experimental investigation include the following:

- Quantify the solubility constants for uranyl and zirconium molybdates.
- Quantify the stability constants of zirconium molybdate species.
- Quantify the steady-state concentration of hydrogen peroxide during reactor operation.
- Quantify the effects of radiolysis on the Eh of the reactor solution.

8 ACKNOWLEDGEMENTS

This report has been created by UChicago Argonne, LLC, Operator of Argonne National Laboratory ("Argonne"). Argonne is managed by UChicago Argonne, LLC, for the U.S. Department of Energy under contract DE-AC02-06CH11357. Work was also supported by the U.S. Department of Energy, National Nuclear Security Administration's (NNSA's) Office of Defense Nuclear Nonproliferation, under Contract DE-AC02-06CH11357.

9 REFERENCES

Gunter Faure, Principles and applications of geochemistry: a comprehensive textbook for geology students, Prentice Hall, 1998, the University of California, 600 pages

Chemical Equilibria in Soils, Willard L. Lindsay, 450 pages, The Blackburn Press (July 31, 2001),

Bard, A. J., R. Parsons, J. Jordan 1985, *Standard Potentials in Aqueous Solution*, Dekker, New York.

Beazley, H., 2008, personal communication from Beazley (Babcock & Wilcox) to G. Vandegrift (Argonne National Laboratory), February 1.

Ferris, L.M., 1961, "Solubility of Molybdic Oxide and its Hydrates in Nitric Acid, Nitric Acid-Ferric Nitrate, and Nitric Acid-Uranyl Nitrate Solutions," *Journal Of Chemical And Engineering Data*, 6: 600–603.

Kubatko, K.H., K.B. Helean, A. Navrotsky, and P.C. Burns, 2003, "Stability of Peroxide-Containing Uranyl Minerals," *Science* 302: 1190–1193.

Martell, A.E., R.M. Smith, and R.J. Motekaitis, 2004, *NIST Standard Reference Database 46*, Version 8.0.

Neely, G., 2008, personal communication from Neeley (Babcock & Wilcox Technical Services Group) to G. Vandegrift (Argonne National Laboratory), January.

Prasad S., and J.V. Barros, 1998, "Electrometric Studies on Uranyl Molybdates as a Function of pH," *Eclética Química* 23: 1–12.

Wolery, T.J., and S.A. Daveler, 1992, EQ6, A Computer Program for Reaction Path Modeling of Aqueous Geochemical Systems: Theoretical Manual, User's Guide, And Related Documentation (Version 7.0), Report UCRL-MA- 110662 PT IV, Lawrence Livermore National Laboratory.

Chemical Science and Engineering Division
Argonne National Laboratory
9700 South Cass Avenue, Bldg. 205
Argonne, IL 60439-4837

www.anl.gov

Argonne National Laboratory is a U.S. Department of Energy
laboratory managed by UChicago Argonne, LLC